



Full Length Article

Sunlight-driven photocatalytic and anticancer properties of biogenic synthesized gold nanoparticles (AuNPs) employing *Polygala elongata*M. Elangovan^a, Murali Santhoshkumar^b, Kumar Selvaraj^{c,d}, Kuppusamy Sathishkumar^{e,*}, Manimaran Kumar^f, Mukesh Kumar Dharmalingam Jothinathan^e, Mansour K. Gatashah^g, Gajendra Kumar Gaurav^h, K. Rajesh^{i,*}^a PG & Research Department of Chemistry, Indian Arts and Science College, Kondam, Tamil Nadu, India^b Department of Biotechnology, Thiruvalluvar University, Serkkadu, Vellore, Tamil Nadu 632 115, India^c Instituto de Desarrollo Tecnológico para la Industria Química (INTEC), CONICET, Ruta Nacional 168, Km. 0, Santa Fe 3000, Argentina^d Facultad de Ingeniería Química, Universidad Nacional del Litoral (UNL), Santiago del Estero 2829, Santa Fe 3000, Argentina^e Center for Global Health Research, Saveetha Medical College and Hospitals, Saveetha Institute of Medical and Technical Sciences (SIMATS), Saveetha University, Chennai, Tamil Nadu 602 105, India^f Research Center for Applied Microbiology, National Research and Innovation Agency (BRIN), Cibinong 16911, Indonesia^g Department of Biochemistry, College of Science, King Saud University, P.O Box 2455, Riyadh 11451, Saudi Arabia^h Schools of Physics and Electronic Information, Yan'an University, Yan'an 716000, Chinaⁱ PG & Research Department of Chemistry, Arignar Anna Govt. Arts College, Cheyyar, Tamil Nadu, India

ARTICLE INFO

Keywords:

AuNPs
PEL extract
Ultrasonic
Antioxidant
Cytotoxicity
Photo catalytic

ABSTRACT

The current study uses an economical and eco friendly method to produce gold (Au) nanoparticles (NPs) using *Polygala elongata* leaf (PEL) extract as a reducing and stabilizing agent. The synthesized materials were characterized using a range of methods, including as BET analysis, TEM-SAED, FT-IR, UV-Vis, and XRD. Biogenic AuNPs' spherical form was shown by SEM and TEM investigations, which also showed that the particles' size range was 10–20 nm, their distribution was homogeneous, and there observed minimal aggregation. The production of biogenic AuNPs was confirmed by the observation of a surface plasmon resonance peak in the absorption spectra, which was detected at 540 nm. Additionally, studies were conducted on the catalytic, cytotoxic, antioxidant, and anticancer characteristics of biogenic AuNPs. The biogenic AuNPs exhibited adaptable applications as a heterogeneous catalyst, achieving percentage degradations of 73 % and 88 % under UV light irradiation, particularly in catalyzing the reduction of Methylene Blue (MeB). Furthermore, the antioxidant properties were evaluated using DPPH free radical scavenging assay in regarding rutin, a widely used antioxidant. With a cytotoxicity value of 500 µg/ml, the produced AuNPs had a strong dose-dependent inhibitory effect on the development of the lung cancer cell line (A549). Therefore, biogenic AuNPs hold potential applications across various research domains, spanning biological and industrial sectors, as well as in the removal of harmful contaminants in water purification.

1. Introduction

Metal-based nanomaterial is growing more and more popular in modern nanomaterial research because of their many uses in fields including biology, wastewater treatment, and catalysis. (Santhoshkumar et al., 2023; Dhandapani et al., 2022 Sathiyaraj et al., 2020). Gold (Au) nanoparticles (NPs) have gained significant attention in this field, being extensively utilized in biotechnology and chemical industries for

applications such as enzyme electrodes, plant biology, catalysis, and cancer treatment (Babu et al., 2020). Over the past decades, numerous researchers possess explored the use of various plant extracts to create potent anti-cancer and anti-microbial agents in clinical trials, with more than 55 % derived from natural sources (Anand et al., 2019). Different methodologies have been created to synthesize metal nanoparticles with specific sizes and shapes (Vijayaraghavan et al., 2017). Biogenic formation of nanoparticles is a rapidly advancing area in nano and

Peer review under responsibility of King Saud University

* Corresponding authors.

E-mail addresses: ksathish570@gmail.com (K. Sathishkumar), krisrajesh1977@gmail.com (K. Rajesh).<https://doi.org/10.1016/j.jksus.2024.103158>

Received 22 December 2023; Received in revised form 3 March 2024; Accepted 6 March 2024

Available online 7 March 2024

1018-3647/© 2024 The Authors. Published by Elsevier B.V. on behalf of King Saud University. This is an open access article under the CC BY-NC-ND license (<http://creativecommons.org/licenses/by-nc-nd/4.0/>).

biotechnology. This method is valued for its non-toxic, biocompatible, and cost-effective nature, playing a pivotal role in advancing environmental technologies for the creation of highly concentrated metals (Annamalai et al., 2021). When comparing the advantages of biogenic synthesis to other biocompatible compounds, such as proteins, peptides, enzymes, and DNA, biogenic synthesis stands out due to its one-step synthesis process, reduced biohazard, ease of improvement, and compatibility with cell culture maintenance (Nazli et al., 2018). Gold nanoparticles (AuNPs) have been prepared using various plants, including *Punica granatum*, *Artemisia capillaries*, and *Couroupita guianensis*, demonstrating catalytic activities and therapeutic potential against lung cancer cell lines (A549) (Lemecho et al., 2022). Among the various green production methods of biogenic AuNPs, ultrasonic-assisted synthesis using *Polygala Elongata* leaf (PEL) extract has gained attention. This method is praised for its low cost, environmental friendliness, and simplicity of use in treating cancer, microbial infections, and breaking down organic contaminants. The PEL extract functioned as a capping and reducing agent. This paper presents the first report on the synthesis and characterization of biogenic ultrasonic-assisted Au NPs, exploring their structural, antioxidant, anticancer properties through in-vitro cytotoxicity assays using MTT against lung cancer cell lines (A549), and catalytic activities under MeB. Additionally, the plausible mechanism of synthesized AuNPs is investigated (El-Deeb et al., 2022; Jadoun et al., 2021; Santhosh et al., 2022; Taha et al., 2022). PEL plants, found in Aazhiyar Forest Research Centre & Medical Farm in Aazhaiyar, Tamilnadu, India, have various medicinal uses, including treating skin conditions, leprosy, and other disorders (Sankaran et al., 2020; Elangovan et al., 2023). Despite its small size, the PEL plant possesses tough bark with deep vertical fissures. The young shoots and leaves are essential in traditional Ayurvedic medicine, belonging to the family Polygalaceae. Specifically, the leaves are used as an anti-rheumatic sedative in Egyptian folk medicine for treating sore throats and whooping cough in children. There are several pharmacological properties related to the plant. including diuretic, anti-inflammatory, cardiogenic, hypoglycemic, laxative, antimicrobial, antihypertensive, and antioxidant properties. Phytochemical compounds found in *Polygala elongata*, including various types of bark and leaf salicortin, saligenin, phenolic glycosides, and pyrocatechol, contribute to its anti-inflammatory properties and inhibition of lung cancer cell lines (A549). Noteworthy phytochemicals noted in the plant include flavonoids, tannins, alkaloids, and terpenoids (Roy et al., 2020; Das et al., 2020; Sun et al., 2023).

2. Experimental section

2.1. Materials

All analytical-grade chemicals were procured from Sigma Aldrich without further purification. *Polygala Elongata* leaves (PEL) were taken from the Aazhiyar Forest Research Centre & Medical Farm, Aazhaiyar, Tamilnadu, India. Gold (III) chloride trihydrate ($\text{HAuCl}_4 \cdot 3\text{H}_2\text{O}$), Potassium Carbonate (K_2CO_3), and Methylene Blue (MeB) were also purchased. Subsequently, all experimental solutions underwent thorough washing with distilled water.

2.2. Extraction of plant material

Fresh *Polygala Elongata* (PEL) leaves were harvested and air-dried using a mixer grinder in the present study. Subsequently, ten ml of distilled water was added to one gram of PEL powder at room temperature. After that, the resulting solutions were sonicated for ten minutes using a 400 W ultrasonic probe. After cooling to ambient temperature for an additional ten minutes, the resulting solution was filtered through whatman filters No.1 to eliminate any remaining biomaterials. For future study, the gathered PEL extract was kept at 4 °C in a dark glass container.

2.3. Extract-based gold nanoparticle synthesis

The synthesis of gold nanoparticles (AuNPs) assisted by *Polygala Elongata* Leaves (PEL) extract was conducted in the presence of gold (III) chloride. In the preparation procedure, a flask was charged with 20 mL of water and 1.5 mL of PEL extract. The pH was adjusted by the gradual addition of a 0.4 M K_2CO_3 solution. Simultaneously, aqueous solution of gold (III) chloride trihydrate ($\text{HAuCl}_4 \cdot 3\text{H}_2\text{O}$) (1.5 mL) was added dropwise to the reaction vessel, which was constantly agitated using a high-powered ultrasonic generator with a gold tip on a magnetic stirrer. To prevent an unwanted photochemical reaction, Aluminium foil was used to cover the reaction vessel. All glassware used in the experiment was washed with HCl and HNO_3 solutions, rinsed using distilled water, and then dried in a 100 °C oven. Subsequently, the produced AuNPs underwent five rounds of centrifugation at 10,000 rpm with deionized water before further characterizations Fig. S1.

2.4. Measurements

Periodically, the absorption spectra were examined using a UV-visible spectrometer (JASCOV-670) covering the range of 200–800 nm. For the purpose to analyse spectrums, three mL of the reaction mixture was taken in a quartz cuvette. Spectral analysis was executed on wavelengths (200 to 800 nm). The potential bio-functionality of AuNPs was determined through FT-IR analysis using a Perkin Elmer spectrometer operating in the 400–4000 cm^{-1} range. An FTIR sample container was filled with the mixture of 250 mg potassium bromide and 2.5 mg dried AuNPs powder. Measurements of X-ray diffraction (XRD) was conducted using a RIGAKU X-ray diffractometer with Cu K radiation, operating in 0-2 θ configurations, and employing parameters of 80 kV and 10 mA. Morphological images were captured using SEM (ZEISS model EVO18) and TEM (FEI-TECNAI G2-20 TWIN with LaB6 filament). BET images of the synthetic samples were obtained using a Gemini and Micrometrics Gemini (2375).

2.5. Efficacy of antioxidants

In a standard procedure, the evaluation of 2,2-diphenyl-2-picrylhydrazyl hydrate (DPPH) was conducted utilizing the procedure proposed by Brand-Williams et al., with particular modifications. The antioxidant properties of the *Polygala Elongata* leaf (PEL) extract were assessed by its ability to neutralize the stable free radical Diphenylpicrylhydrazine (DPPH). Measurements were taken at 517 nm using a spectrophotometer to observe the color change from purple to yellow. For the evaluation, various concentrations (100–400 $\mu\text{g}/\text{mL}$) of the PEL extract, along with gold nanoparticles (AuNPs), were individually mixed with 3 mL of 0.1 mmol Rutin as a standard. Without the sample, a control was made with DPPH methanol reagent. The DPPH solution was incubated in the dark for 15 min and then thoroughly mixed. Room temperature was maintained for the reaction mixture in the dark for an additional 30 min. The absorbance was spectrophotometrically quantified at 517 (nm). The following formula was used to calculate the plant extract's scavenging ability.

$$(\text{DPPH})\text{Scavenging activity}(\%) = [(Ac - As)/Ac] \times 100$$

2.6. Anticancer activity

In the present investigation, live cells undergo a transformation where the salt of formazon is generated during the conversion of 2-(4,4-dimethyl-2-tetrazoyl)-2,5-diphenyl-2,4-tetrazolium (MTT) into its derivative. The production of formazon serves as the quantifiable indicator of the number of live cells. Subsequently, the solubilized formazon is assessed for cell viability using a microplate reader. For this purpose, MTT (50 mL) and 100 mL of treated cells were incubated at 37 °C for 3 h. After the incubation period, 200 μl of PBS was added to all samples, and

any excess MTT was carefully aspirated off. Following this, 200 μ l of acid-propanol was added for solubilization, and the samples were overnight left in the dark. The absorbance was measured at 650 nm using a microplate reader (Bio RAD U.S.A.).

2.7. Photo catalytic activity

$$\eta = \left(1 - \frac{C}{C_0}\right) \times 100$$

The reacting suspensions were produced by adding 600 mg of catalyst to 600 mL of a Methylene Blue (MeB) solution, which had an initial concentration of 3.9×10^{-3} mol/L, in accordance with normal protocol. To create an adsorption–desorption equilibrium between the MeB molecules, the catalyst and the aqueous solution of MeB were shaken in total darkness before the photocatalytic run began. Notably, the synthesized sample did not exhibit any color change when exposed to UV radiation in the absence of gold (Au). Consequently, both irradiation and the presence of Au NPs were necessary for effective degradation. At regular intervals, samples were taken from the suspension, subjected to centrifugation, and filtered. At room temperature, the concentration of MeB in each sample was assessed using a UV–Vis spectrophotometer that had a wavelength of 670 nm. The given formula was used to determine the deterioration percentage.

The concentration (C) is defined as the MeB concentration after a specific duration of exposure, while C_0 represents the MeB concentration before illumination. The production of AuNPs using the following procedure allowed for determining the Chemical Oxygen Demand (COD) of the MeB dye solution. A predetermined volume of standard potassium dichromate ($K_2Cr_2O_7$), silver sulfate ($AgSO_4$), and sulfuric acid (H_2SO_4) was refluxed with samples for 2 h, and the reaction was titrated with standard ferrous ammonium sulfate (FAS) using mercury sulfate ($HgSO_4$) as an indicator. De-ionized water served as a blank titration in place of the MeB dye sample. The COD of the MeB dye solution was calculated using the provided equation.

3. Results and discussion

3.1. UV visible evaluation

Recently generated metal nanoparticles have attracted a great attention. As they are inexpensive and nontoxic in the medical field. The synthesis of AuNPs and *Polygala elongata* occurs in the present study, and the solution takes on a ruby-red color to signify the production of AuNPs using plant extract. The UV–visible spectra of biogenic

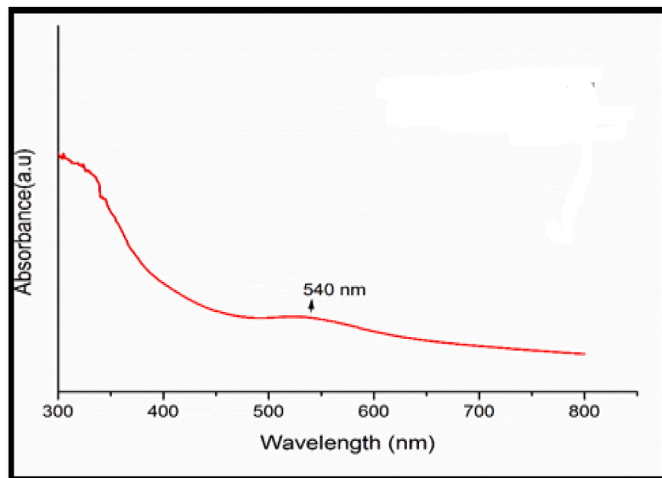


Fig. 1. AuNPs UV–visible Spectra.

ultrasonic-assisted AuNPs using PEL extract are presented in Fig. 1 The absorption spectra exhibit a peak at 540 nm, attributed to the surface plasmon resonance (SPR), confirming the blue shift and formation of AuNPs (Vinayagam et al., 2021). The vibrational peaks of SPR are associated with color changes, ranging from yellow to dark brown, at temperatures of 40 and 80 °C, indicating the influence of shape and size. This color transition serves as significant evidence for the reduction of $HAuCl_4$ from Au^{3+} to Au^0 .

In Fig. 1 a weak SPR band is observed with oversized particles, indicating a low conversion of Au^{3+} to AuNPs at 40 min. However, extending the reduction time to 80 min results in an increased SPR band. The coating of PEL extract molecules and reduction of Au ions contribute to a reduced particle diameter. Although the reaction time is prolonged, it does not significantly alter the SPR bands, indicating that the optimal contact time for producing homogeneous AuNPs is up to 80 min. As a result, PEL extract acts as a stabilizing and decreasing agent during the AuNP extraction procedure.

3.2. FT-IR analysis

The spectrum of FT-IR of biogenic ultrasonic-enabled AuNPs using PEL extract is depicted in Fig. 2(a-b). In the FT-IR spectra, absorption bands were observed at 3313 cm^{-1} , 2929 cm^{-1} , 1608 cm^{-1} , 1404 cm^{-1} , 1328 cm^{-1} , 1078 cm^{-1} , 931 cm^{-1} , 904 cm^{-1} , and 596 cm^{-1} for PEL extract, and at 3286 cm^{-1} , 1577 cm^{-1} , 1413 cm^{-1} , 1325 cm^{-1} , 1097 cm^{-1} , and 840 cm^{-1} for AuNPs. These bands are attributed to various functional groups, such as the amide links of proteins, carbonyl stretch, and free N–H stretch vibrations, as evidenced by peaks at 3313 cm^{-1} , 2929 cm^{-1} , and 1608 cm^{-1} . Amino acid residues and peptides with carbonyl groups have a strong affinity for metal binding. This interaction forms a protective layer of proteins around gold nanoparticles, preventing aggregation and stabilizing the particles.

In addition, FT-IR scanning is noted to examine the functional groups and physicochemical characteristics involved in the synthesis of *Polygala elongata*. The characteristic bands at 1413 cm^{-1} and 1404 cm^{-1} indicate the presence of (C–O) stretching vibrations of phenolic glycosides. Additionally, a band at 1328 cm^{-1} to 1325 cm^{-1} suggests the presence of C–CO–C stretching vibrations of alkyl ketones in carbonyl compounds. Bands at 1097 cm^{-1} and 1074 cm^{-1} are attributed to =CH₂ vibrations and –C–N stretching, predominantly found in polysaccharides. The band at 931 cm^{-1} indicates the presence of mono-substituted alkenes in alkaloids (Sathiyaraj et al., 2021). Similarly, bands from 904 cm^{-1} to 840 cm^{-1} showed C–H out-of-plane bending in di-substituted benzene ring vibrations of cardiac glycosides. Considering the composition of PEL, which includes alkaloids, flavonoids, minerals, amino acids, sterols, glycosides, and phenolics, these constituents likely contribute to the observed FT-IR spectrum.

3.3. XRD screening

The XRD analysis of biogenic ultrasonic-assisted AuNPs utilizing PEL extract is shown in Fig. 3(a-c). The face-centered cubic (FCC) crystalline structure of AuNPs is indicated by the major diffraction peaks observed at 28.27 , 38.81 , 40.91 , 45.45 , 50.51 , 56.84 , 59.11 , 66.69 , and 74.29 , respectively, which are indexed to the (220), (311), (111), (200), (321), (211), and (220) crystallographic planes. (JCPDS File No. 01–089–3697) (Pitchai et al., 2022).

The absence of additional peaks in the spectra indicates the absence of impurities, confirming the essentially crystalline nature of biogenic AuNPs. Additionally, the PEL leaf extract contained a variety of chemicals, which led to the observation of unassigned diffraction peaks. Utilizing the Debye-Scherrer equation, the average crystallite size of biogenic AuNPs was ascertained.

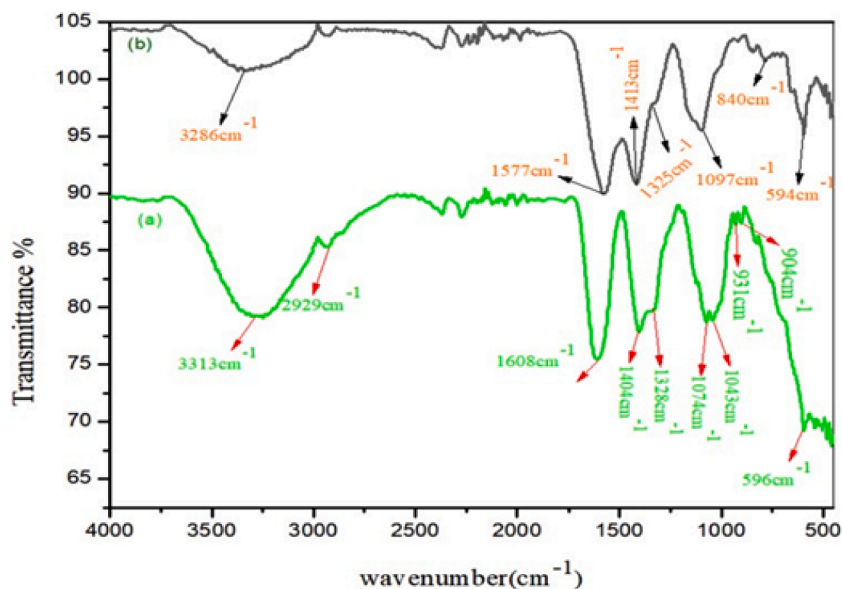


Fig. 2. FTIR spectra of Au NPs.

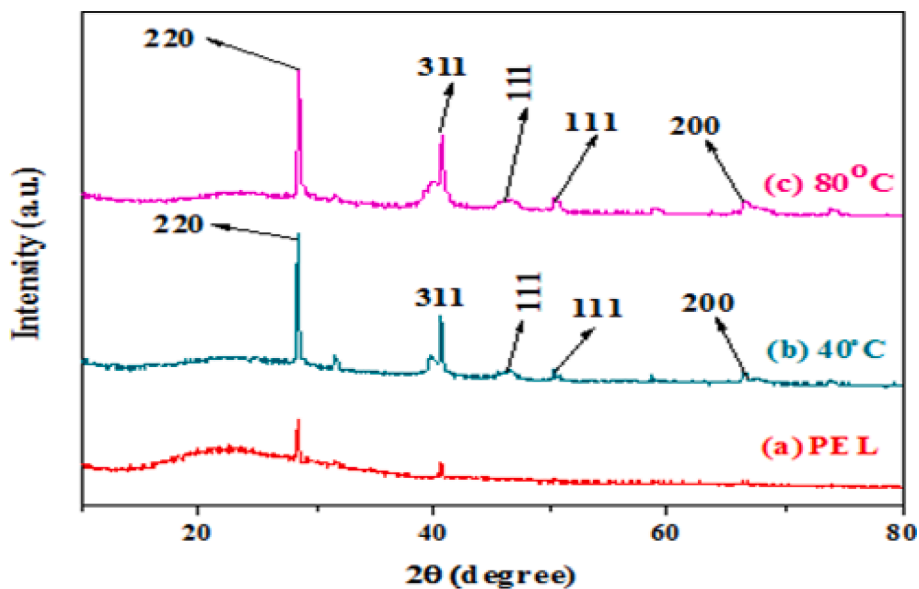


Fig. 3. XRD pattern of Au NPs.

3.4. Scanning electron microscopy (SEM)

The SEM of biogenic ultrasonic assisted AuNPs utilizing PEL as extract is shown in (Fig. 4). In the nanoscale range, it exhibited a

spherical-like morphology around (100–50 μm), respectively. We conclude that it can play a significant part in the formation of smaller particles in PEL extract.

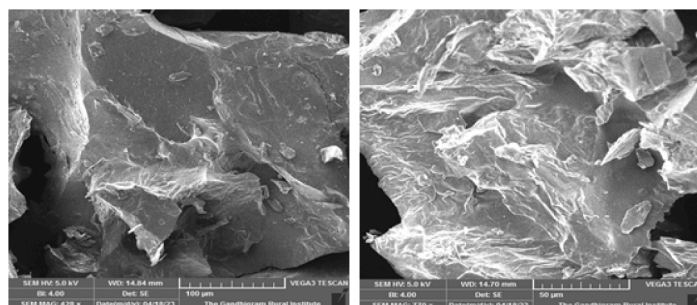


Fig. 4. SEM of Au NPs.

3.5. TEM analysis

TEM-SAED investigation of biogenic ultrasonic-assisted AuNPs utilizing PEL extract is shown in Fig. 5(a-d). The particles round shape indicates that their diameters range from 100 to 5 nm. The formation of smaller-sized AuNPs during the process is attributed to hydrogen bonding and the exchange of electrons between the biomolecules of PEL extracts capping with Au⁰.

In Fig. 5(d), the SAED patterns display two rings, indicating the crystalline nature of the synthesized samples. These rings correlate with the 200 & 220 planes of the face-centered cubic crystalline lattice, aligning well with the XRD data (Gao et al., 2022).

3.6. Isotherms for nitrogen adsorption–desorption

The N₂ adsorption–desorption isotherms for biogenic ultrasonic-assisted Au NPs, utilizing PEL as an extract, are presented in (Fig. 6 a-b). The calculated surface area and pore volume from the isotherm were determined to be 47 m²g⁻¹ and 106 m²g⁻¹, 0.16 cm³g⁻¹ and 0.43 cm³g⁻¹, respectively. The corresponding pore size distribution exhibits a broad range at (14–25) & (10–16) nm. The increase in the surface area of synthesized AuNPs at 800 °C is attributed to the reduction in particle size (Zhou et al., 2022).

3.7. Graph showing synthetic Au NPs' radical scavenging activity against DPPH

The DPPH free radical scavenging experiment, depicted in (Fig. 7), was conducted to evaluate the antioxidant capacity of the synthesized AuNPs. Our study revealed that both the PEL extract and artificial AuNPs exhibited radical scavenging activity. However, in comparison to PEL extract (63.4 %), Rutin control (60 %), and AuNPs (75.2 %), these three substances demonstrated the lowest free radical scavenging activity (Baliyan et al., 2022). The presence of substances that are bioactive within the PEL extract may contribute to its potential antioxidant role. Furthermore, the enhanced antioxidant activity of AuNPs is attributed to the adsorption of existing bioactive components from the fruit extract onto the spherical NPs with a higher surface area. Interactions between plant metabolites and metal ions during nanoparticle

production may lead to molecules that are more effective in scavenging free radicals. Additionally, electrostatic interactions between positively (+vely) or neutrally charged AuNPs and negatively (-vely) charged phytochemicals enhance the bioactivity of plants. Previous studies have indicated a progressive increase in antioxidant activity as treatment doses are elevated (Monika et al., 2022).

3.8. AuNPs cell viability as assessed by the MTT assay

As depicted in (Fig. 8), the generated AuNPs were systematically assessed in a dose-dependent manner for the lung cancer cell line A549. A reduction in cell viability was observed with increasing concentrations of administered dosages during a 24-hour exposure. Treatment with AuNPs for 24 h resulted in a decrease in the viability of lung cancer cells to 38 % at 500 µg/mL, 42.07 % at 400 µg/mL, 43.96 % at 300 µg/mL, 51.69 % at 200 µg/mL, and 59.24 % at 100 µg/mL (Soares et al., 2023). Concurrently, a rise in AuNPs concentrations revealed substantial cellular morphological damage, including a suggestive decrease in cell number, cell shrinkage, and diminished cell-to-cell interaction. These results demonstrate AuNPs cytotoxic activity against cancer cells, which is dose-dependent. Although the exact mechanism of NPs cytotoxicity on lung cancer cells is still being studied, it is thought that the particles' small size makes it easier for them to enter cancer cells and target specific cellular components. Furthermore, NPs can be designed to deliver specific drugs or therapeutic agents directly to cancer cells, which can improve their efficacy and lessen the negative effects of conventional chemotherapy medicines.

Previous reports suggest that AuNPs can penetrate cells and inhibit their growth by disrupting double-stranded DNA molecules. The release of Au ions from AuNPs is believed to induce interactions between DNA, mitochondria, and nucleases, ultimately leading to cellular death. Earlier studies on mammalian cancer cells have shown that platinum nanoparticles predominantly target DNA molecules, causing DNA fragmentation (Wei et al., 2024; Naraginti et al., 2016). Notably, normal human cells demonstrated resilience to the biogenically synthesized AuNPs without discernible harm. The enhanced anti-cancer effects and reduced cytotoxicity to healthy cells offered by biogenic AuNPs hold great promise for cancer cell therapy (Fig. 9 a-b). Additionally, the cost-effectiveness of biogenic AuNPs production can potentially lower treatment expenses (Tabatabaie et al., 2022; Naraginti et al., 2014).

3.9. AuNPs degradation as described by MeB

In the current investigation, the photo catalytic efficacy of biogenically assisted Au NPs using PEL extract was quantified by monitoring the photodecomposition of MeB pollutants under UV light exposure, as illustrated in (Fig. 10). The reduction in MeB's absorbance spectra occurred at 670 nm at irregular intervals (Gloria et al., 2023; Singh et al., 2022). In the initial blank experiment, the catalytic activity of only H₂O₂ was assessed in the absence of an Au catalyst, revealing that H₂O₂ does not actively participate in the degradation of MeB. With the Au catalyst present, MeB degradation was observed within approximately 50 min, dependent on the capacity to distinguish between the electron-hole pair and secondary processes that occur when electrons recombine, causing to the degradation of dye molecules (Palajonnala Narasaiah et al., 2022).

4. Conclusion

In this investigation, PEL, a non-toxic material, was used to produce biogenic ultrasonically aided AuNPs. This ultrasonic method's dependability, affordability, and environmental friendliness make it significantly superior than conventional techniques. The size, shape, and optical property of the produced AuNPs were evaluated using a variety of methods. A surface plasmon resonance band at 540 nm was visible in the absorption spectra, indicating that the AuNPs had been produced

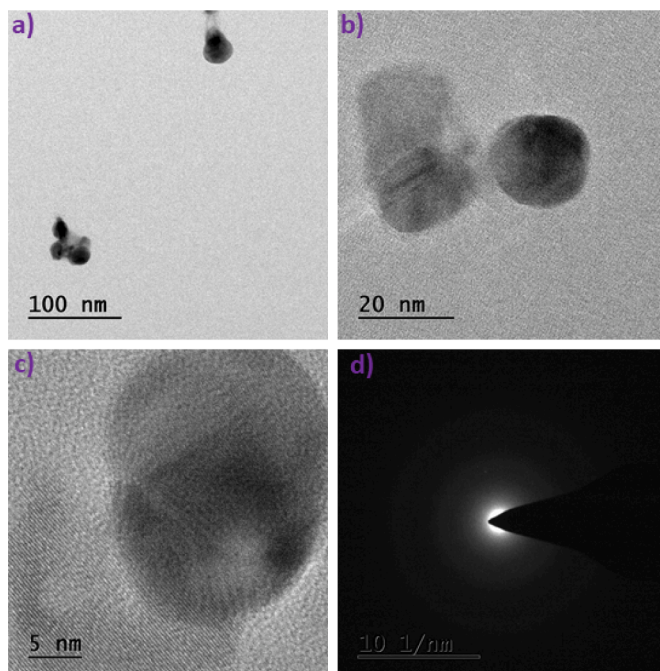


Fig. 5. TEM-SAED patterns of Au NPs.

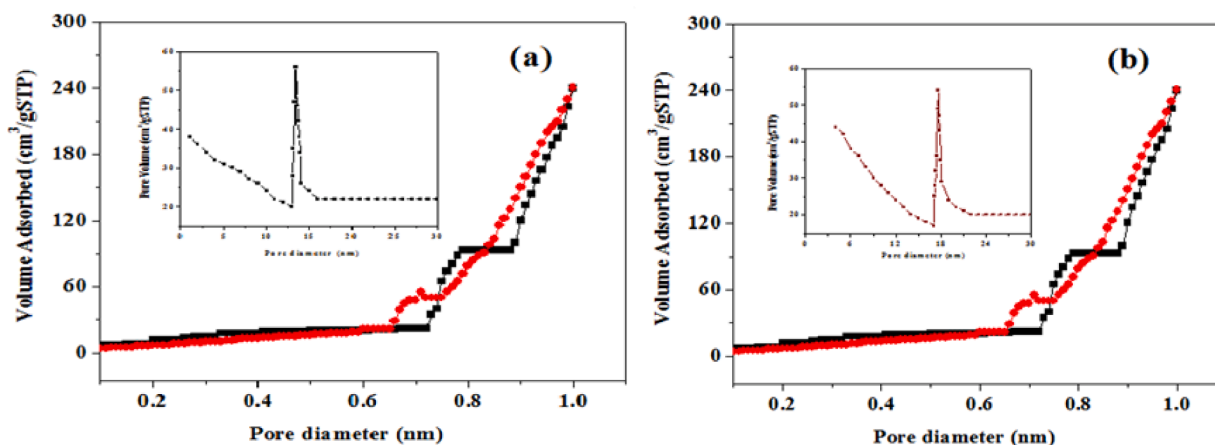


Fig. 6. BET images of Au NPs.

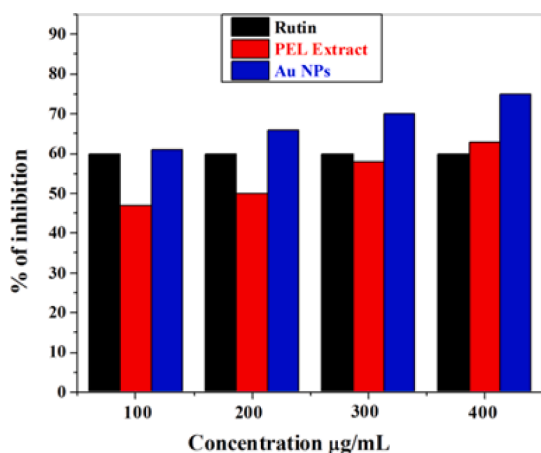


Fig. 7. Graph showing synthetic Au NPs' radical scavenging activity against DPPH.

successfully. Subsequent analyses using XRD, SEM, and TEM-SAED verified that the biogenic ultrasonically aided AuNPs are crystalline. The SEM and TEM studies exhibited a spherical-like shape with an

average diameter of 100 nm–5 nm. Utilizing the lung cancer cell line A549 in the MTT assay, the pharmacological properties of PEL extract were harnessed to activate the anticancer activity of the newly produced biogenic ultrasonically assisted AuNPs, eliminating the need for metal molecule doping. In degradation experiments, the biogenic assisted AuNPs displayed high catalytic efficiency, particularly at 80 °C, leading to the mineralization of MeB. These biogenic ultrasonically assisted AuNPs have numerous benefits that can be applied to a wide number of fields, such as wastewater treatment, cancer treatment, agricultural, green industrial processes, environmental bioremediation, and more. As a result, they are highly adaptable and suggest great potential in a variety of fields.

Credit authorship contribution statement

M. Elangovan: Writing – original draft, Investigation, Validation, Formal analysis. **Murali Santhoshkumar:** Formal analysis, Methodology. **Kumar Selvaraj:** Writing – review & editing. **Kuppusamy Sathishkumar:** Writing – review & editing, Resources. **Manimaran Kumar:** Writing – review & editing. **Mukesh Kumar Dharmalingam Jothinathan:** Writing – review & editing. **Mansour K. Gatasheh:** Funding acquisition, Project administration, Software. **Gajendra Kumar Gaurav:** Visualization, Review & editing. **K. Rajesh:** Writing –

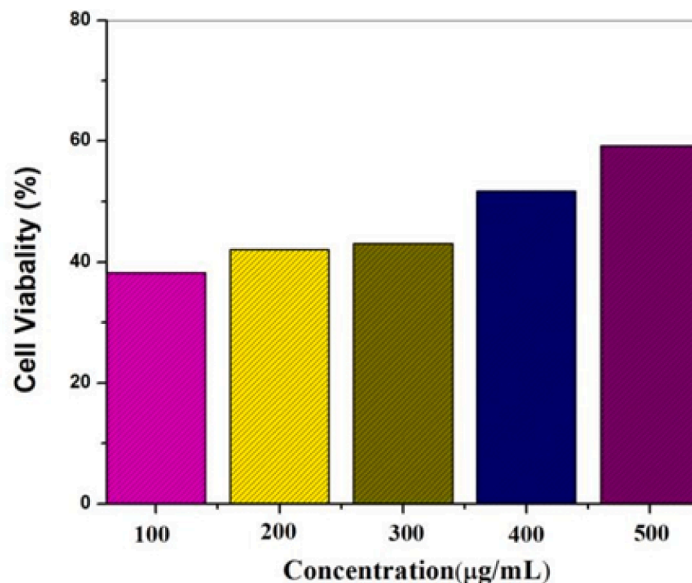


Fig. 8. Au NPs cell viability as assessed by the MTT assay.

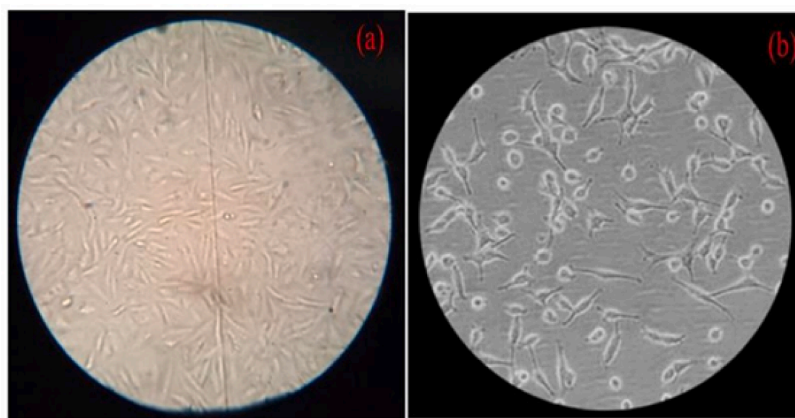


Fig. 9. Effect of AuNPs on cancer cells' cellular shape at varying concentrations: (a) Control; (b) Maximum cells exposed at 500 µg/mL.

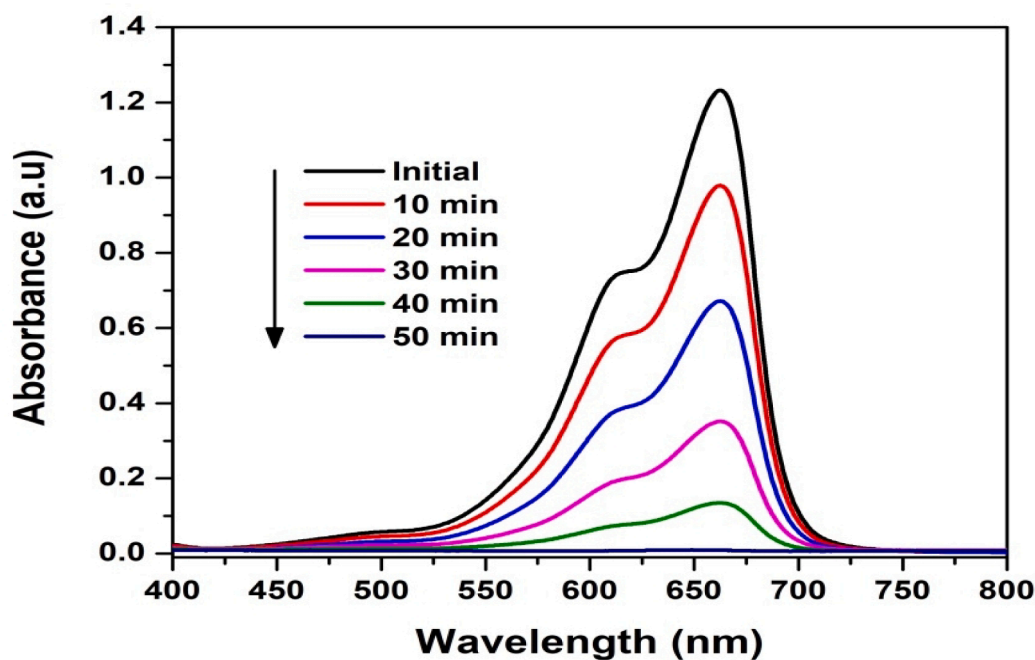


Fig. 10. AuNPs degradation as described by MeB.

review & editing, Visualization, Supervision.

Declaration of competing interest

The authors declare that they have no known competing financial interests or personal relationships that could have appeared to influence the work reported in this paper.

Acknowledgments

The authors extend their appreciation to the Researchers Supporting Project number (RSP2024R393), King Saud University, Riyadh, Saudi Arabia.

Appendix A. Supplementary material

Supplementary data to this article can be found online at <https://doi.org/10.1016/j.jksus.2024.103158>.

References

- Anand, U., Jacobo-Herrera, N., Altemimi, A., Lakhssassi, N., 2019. A comprehensive review on medicinal plants as antimicrobial therapeutics: potential avenues of biocompatible drug discovery. *Metabolites* 9 (11), 258. <https://doi.org/10.3390/metabo9110258>.
- Annamalai, J., Ummalyma, S.B., Pandey, A., Bhaskar, T., 2021. Recent trends in microbial nanoparticle synthesis and potential application in environmental technology: a comprehensive review. *Envir. Sci. Pollu. Res.* 28, 49362–49382. <https://doi.org/10.1007/s11356-021-15680>.
- Babu, B., Palanisamy, S., Vinosha, M., Anjali, R., Kumar, P., Pandi, B., Tabarsa, M., You, S., Prabhu, N.M., 2020. Bioengineered gold nanoparticles from marine seaweed *Acanthophora spicifera* for pharmaceutical uses: antioxidant, antibacterial, and anticancer activities. *Biopro. Biosyst. Eng.* 43, 2231–2242. <https://doi.org/10.1007/s00449-020-024083>.
- Baliyan, S., Mukherjee, R., Priyadarshini, A., Vibhuti, A., Gupta, A., Pandey, R.P., Chang, C.M., 2022. Determination of antioxidants by DPPH radical scavenging activity and quantitative phytochemical analysis of *Ficus religiosa*. *Molecules* 27 (4), 1326. <https://doi.org/10.3390/molecules27041326>.
- Das, R.N., Balupillai, A., David, E., Santhoshkumar, M., Muruhan, S., 2020. Naringin, a natural flavonoid, modulates UVB radiation-induced DNA damage and photoaging by modulating NER repair and MMPs expression in mouse embryonic fibroblast cells. *J. Environ. Pathol. Toxicol. Oncol.* 39 (2) <https://doi.org/10.1615/JEnvironPatholToxicolOncol.2020031914>.

- Dhandapani, P., Santhoshkumar, M., Narenkumar, J., AlSalhi, M.S., Kumar, P.A., Devanesan, S., Kokilaramani, S., Rajasekar, A., 2022. Bio-approach: preparation of RGO-AgNPs on cotton fabric and interface with sweat environment for antibacterial activity. *Biopro. Biosyst. Eng.* 45 (11), 825–1837. <https://doi.org/10.1007/s00449-022-02789-7>.
- Elangovan, M., Rajesh, K., Santhoshkumar, M., Sathishkumar, K., Bharathiraja, N., Gnanasri, M., 2023. Exploring the potential of agro-waste-mediated silver nanoparticles as antibacterial and antioxidant agents. *Biomass Convers. Biorefin.* 23, 1. <https://doi.org/10.1007/s13399-023-04945-9>.
- El-Deeb, N.M., Khattab, S.M., Abu-Youssef, M.A. and Badr, A.M., 2022. Green synthesis of novel stable biogenic gold nanoparticles for breast cancer therapeutics via the induction of extrinsic and intrinsic pathways. *Sci. Rep.* 12(1), 11518. doi:41598-022-15648-y.
- Gao, L., Mei, S., Ma, H., Chen, X., 2022. Ultrasound-assisted green synthesis of gold nanoparticles using citrus peel extract and their enhanced anti-inflammatory activity. *Ultras. Sono. Chem.* 83, 105940 <https://doi.org/10.1016/j.ulsonch.2022.105940>.
- Gloria, D.C.S., Brito, C.H.V., Mendonça, T.A.P., Brazil, T.R., Domingues, R.A., Vieira, N. C.S., Santos, E.B., Gonçalves, M., 2023. Preparation of TiO₂/activated carbon nanomaterials with enhanced photocatalytic activity in paracetamol degradation. *Mater. Chem. Phys.* 305, 127947 <https://doi.org/10.1016/j.matchemphys.2023.127947>.
- Jadoun, S., Arif, R., Jangid, N.K., Meena, R.K., 2021. Green synthesis of nanoparticles using plant extracts: A review. *Env. Chem. Lett.* 19, 355–374. <https://doi.org/10.1007/s10311-020-01074x>.
- Lemecho, B.A., Sabir, F.K., Andoshe, D.M., Gultom, N.S., Kuo, D.H., Chen, X., Mulugeta, E., Desissa, T.D., Zelekew, O.A., 2022. Biogenic synthesis of Cu-doped ZnO photocatalyst for the removal of organic dye. *Bio. Chem. Appl.* 2022, 1–10. <https://doi.org/10.1155/2022/8081494>.
- Monika, P., Chandraprabha, M.N., Hari Krishna, R., Vittal, M., Likhitha, C., Pooja, N., Chaudhary, V., 2022. Recent advances in pomegranate peel extract mediated nanoparticles for clinical and biomedical applications. *Biotech. Genetic. Eng. Rev.* 1, 29. <https://doi.org/10.1080/02648725.2022.2122299>.
- Naraginti, S., Sivakumar, A., 2014. Eco-friendly synthesis of silver and gold nanoparticles with enhanced bactericidal activity and study of silver catalyzed reduction of 4-nitrophenol. *Spectro. Acta Part A: Mol. Bio Spec.* 128, 357–362. <https://doi.org/10.1016/j.saa.2014.02.083>.
- Naraginti, S., Li, Y., Wu, Y., 2016. A visible light mediated synergistic catalyst for effective inactivation of E. coli and degradation of azo dye direct Red-22 with mechanism investigation. *RSC. Adv.* 6, 75724–75735. <https://doi.org/10.1039/C6RA16141C>.
- Nazli, A., Baig, M.W., Zia, M., Ali, M., Shinwari, Z.K., Haq, I.U., 2018. Plant-based metallic nanoparticles as potential theranostics agents: bioinspired tool for imaging and treatment. *IET Nanobiotech.* 12 (7), 869–878. <https://doi.org/10.1049/ietnbt.2017.0325>.
- Palajonnala Narasaiah, B., Banoth, P., Bustamante Dominguez, A.G., Mandal, B.K., Kumar, C.K., Barnes, C.H., De Los Santos Valladares, L. and Kollu, P., 2022. Biogenic Photo-Catalyst TiO₂ Nanoparticles for Remediation of Environment Pollutants. *ACS omega*, 7(30), 26174–26189. doi:10.1021/acsomega.2c01763.
- Pitchai, P., Subramani, P., Selvarajan, R., Sankar, R., Vilwanathan, R., Sibanda, T., 2022. Green synthesis of gold nanoparticles (AuNPs) using *Caulerpa racemosa* and evaluation of its antibacterial and cytotoxic activity against human lung cancer cell line. *Arab. J. Basic. Appl. Sci.* 29 (1), 351–362. <https://doi.org/10.1080/25765299.2022.2127510>.
- Sankaran, V., Murali, S.K., Ghidan, A., Al Antary, T., David, E., 2020. Oral cancer preventive potential of polydatin: A nanoencapsulation approach. *J. Phytol.* 12, 109–116. <https://doi.org/10.25081/jp.2020.v12.6618>.
- Santhosh, P.B., Genova, J., Chamati, H., 2022. Green synthesis of gold nanoparticles: An eco-friendly approach. *Chemistry* 4 (2), 345–369. <https://doi.org/10.3390/chemistry4020026>.
- Santhoshkumar, M., Perumal, D., Narenkumar, J., Ramachandran, V., Muthusamy, K., Alfarhan, A., David, E., 2023. Potential use of bio functionalized nanoparticles to attenuate triple negative breast cancer (MDA-MB-231 cells). *Biopro. Biosyst. Eng.* 46 (6), 803–811. <https://doi.org/10.1007/s00449-023-02858-5>.
- Sathiyaraj, S., Suriyakala, G., Gandhi, A.D., Saranya, S., Santhoshkumar, M., Kavitha, P., Babujanathanam, R., 2020. Green biosynthesis of silver nanoparticles using vallarai chooranam and their potential biomedical applications. *J. Inorg. Organomet. Poly Mater.* 30, 4709–4719. <https://doi.org/10.1007/s10904-020-01683-7>.
- Sathiyaraj, S., Suriyakala, G., Gandhi, A.D., Babujanathanam, R., Almaary, K.S., Chen, T.W., Kaviyarasu, K., 2021. Biosynthesis, characterization, and antibacterial activity of gold nanoparticles. *J. Infect. Pub. Health* 14 (12), 1842–1847. <https://doi.org/10.1016/j.jiph.2021.10.007>.
- Singh, A.R., Dhumal, P.S., Bhakare, M.A., Lokhande, K.D., Bondarde, M.P., Some, S., 2022. In-situ synthesis of metal oxide and polymer decorated activated carbon-based photocatalyst for organic pollutants degradation. *Separat. Purif. Tech.* 286, 120380 <https://doi.org/10.1016/j.seppur.2021.120380>.
- Soares, S., Faria, I., Aires, F., Monteiro, A., Pinto, G., Sales, M.G., Correa-Duarte, M.A., Guerreiro, S.G., Fernandes, R., 2023. Application of gold nanoparticles as radiosensitizer for metastatic prostate cancer cell lines. *Inter. J. Mol. Sci.* 24 (4), 4122. <https://doi.org/10.3390/ijms24044122>.
- Sun, W., Shahrajabian, M.H., 2023. Therapeutic potential of phenolic compounds in medicinal plants—Natural health products for human health. *Molecules* 28 (4), 1845. <https://doi.org/10.3390/molecules28041845>.
- Tabatabaie, F., Franich, R., Feltis, B., Geso, M., 2022. Oxidative damage to mitochondria enhanced by ionising radiation and gold nanoparticles in cancer cells. *Inter. J. Mol. Sci.* 23 (13), 6887. <https://doi.org/10.3390/ijms23136887>.
- Taha, R.H., 2022. Green synthesis of silver and gold nanoparticles and their potential applications as therapeutics in cancer therapy; a review. *Inorg. Chem. Commun.* 143, 109610 <https://doi.org/10.1016/j.inoche.2022.109610>.
- Vijayaraghavan, K., Ashokkumar, T., 2017. Plant-mediated biosynthesis of metallic nanoparticles: A review of literature, factors affecting synthesis, characterization techniques and applications. *J. Environ. Chem. Eng.* 5 (5), 4866–4883. <https://doi.org/10.1016/j.jece.2017.09.026>.
- Vinayagam, R., Santhoshkumar, M., Lee, K.E., David, E., Kang, S.G., 2021. Bioengineered gold nanoparticles using *Cynodon dactylon* extract and its cytotoxicity and antibacterial activities. *Bio. Biosys. Eng.* 44, 1253–1262. <https://doi.org/10.1007/s00449-021-02527-5>.
- Wei, X., Naraginti, S., Yang, X., Xu, X., Li, J., Zhu, M., Chen, P., Jiang, P., 2024. Simultaneous degradation of SMX for efficient nitrogen fixation to ammonia and hydrogen evolution using AgVO₃@ rGO-Ag₃PO₄ (110) heterojunction. *Int. J. Hyd. Ene.* 56, 629–641. <https://doi.org/10.1016/j.ijhydene.2023.12.162>.
- Zhou, Y., Yuan, Y., Cong, S., Liu, X., Wang, Z., 2022. N₂-selective adsorbents and membranes for natural gas purification. *Separat. Purific. Tech.* 300, 121808 <https://doi.org/10.1016/j.seppur.2022.121808>.